



OPEN HIV-1 Vpu protein forms stable oligomers in aqueous solution via its transmembrane domain self-association

Saman Majeed^{1,6}, Lan Dang^{2,6}, Md Majharul Islam¹, Olamide Ishola¹, Peter P. Borbat³, Steven J. Ludtke⁴✉ & Elka R. Georgieva^{1,5}✉

We report our findings on the assembly of the HIV-1 protein Vpu into soluble oligomers. Vpu is a key HIV-1 protein. It has been considered exclusively a single-pass membrane protein. Previous observations show that this protein forms stable oligomers in aqueous solution, but details about these oligomers still remain obscure. This is an interesting and rather unique observation, as the number of proteins transitioning between soluble and membrane embedded states is limited. In this study we made use of protein engineering, size exclusion chromatography, cryoEM and electron paramagnetic resonance (EPR) spectroscopy to better elucidate the nature of the soluble oligomers. We found that Vpu oligomerizes via its N-terminal transmembrane domain (TM). CryoEM suggests that the oligomeric state most likely is a hexamer/heptamer equilibrium. Both cryoEM and EPR suggest that, within the oligomer, the distal C-terminal region of Vpu is highly flexible. Our observations are consistent with both the concept of specific interactions among TM helices or the core of the oligomers being stabilized by hydrophobic forces. While this study does not resolve all of the questions about Vpu oligomers or their functional role in HIV-1 it provides new fundamental information about the size and nature of the oligomeric interactions.

The HIV-1 encoded Vpu protein fulfils important functions, aiding virus adaptation and proliferation^{1–6}. Despite its small size of about 80 amino acids (aa), the protein has a multi-domain organization and participates in diverse interactions with cellular components. It consists of a short soluble N-terminus followed by what is believed a transmembrane Helix 1 (TM), and two soluble helices, Helix 2 and Helix 3, in the C-terminal domain (Fig. 1)^{5,7–9}. Membrane-associated Vpu spans the membrane bilayer through its TM Helix 1. It resides and functions in the plasma membrane (PM) and endomembranes of infected cell and forms a homo-oligomer (believed to be a pentamer) in the membranes of Golgi and intracellular vesicles, but not in the endoplasmic reticulum (ER)^{10–13}. Monomeric Vpu associates with human tetherin (BST2 protein) in PM via TM Helix 1 forming a Vpu-tetherin complex, leading to enhancement of tetherin ubiquitination and its trafficking for degradation^{14,15}. Therefore, when associated with cellular membranes, this protein appears to exist in several functional quaternary structures. Recently, we found that in addition to membrane-bound self-association, full-length (FL) Vpu also forms homo-oligomers in aqueous solution outside a lipid/hydrophobic environment¹⁶ which may significantly broaden its role in the HIV lifecycle, as soluble transport between membranes now needs to be considered.

Although, Vpu self-association in solution has been previously observed¹⁰, no further characterization of the oligomers was performed. In our previous study, we used analytical size exclusion chromatography (SEC), negative staining electron microscopy (nsEM) with 2-D analysis and electron paramagnetic resonance (EPR) spectroscopy, revealing that the oligomers are rather stable and uniform at protein concentrations of and above 5 μM ¹⁶. This was an interesting result, given that the prevailing opinion is that Vpu is exclusively a transmembrane protein. Furthermore, a previous study found that soluble Vpu oligomers form even upon the expression of this

¹Department of Chemistry and Biochemistry, Texas Tech University, Lubbock, TX 79409, USA. ²Graduate Program in Quantitative and Computational Biosciences, Graduate School of Biomedical Sciences at Baylor College of Medicine, Houston, TX, USA. ³Department of Chemistry and Chemical Biology and ACERT, Cornell University, Ithaca, NY 14853, USA. ⁴Department of Biochemistry and Molecular Pharmacology, Baylor College of Medicine, Houston, TX 77030, USA. ⁵Center for Membrane Protein Research, TTU Health Science Center, Lubbock, TX 79430, USA. ⁶These authors contributed equally: Saman Majeed and Lan Dang. ✉email: sludtke@bcm.edu; elgeorgi@ttu.edu

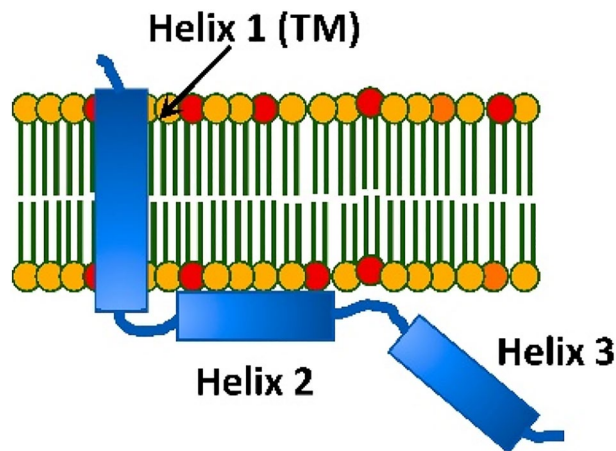


Figure 1. A cartoon representation of the topology of HIV-1 Vpu in lipid membranes: Vpu traverses the membrane via its hydrophobic Helix 1 (TM helix). Helix 2 is membrane-associated; however, other model of Helix 2 not making a contact with the membrane surface was also proposed.

protein in a rabbit reticulocyte lysate¹³, which furthers the concept of a possible physiological role of soluble Vpu oligomers. It may be that the protein is even more functionally versatile than its current known physiological roles, because of its capacity to transition from soluble to membrane-bound form. Several other unconventional transmembrane proteins from eukaryotic and prokaryotic organisms are known to exist and function in both soluble and membrane-bound states, e.g., the members of Bcl-2 family¹⁷, anti-bacterial toxins¹⁸, etc. suggesting that this mechanism could apply to Vpu as well.

It is challenging to study the structure of small oligomers like Vpu due to their size and potential heterogeneity in solution. To aid in these studies we made use of the MBP-Vpu construct developed previously¹⁶. The MBP domain is sufficiently large and stable that it can be directly observed in cryoEM, and used as a tag for counting the number of self-associated Vpu molecules in each oligomer. The same oligomers were also studied using SEC, continuous wave electron paramagnetic resonance (CW EPR) and double electron–electron resonance (DEER) spectroscopy. While still an incomplete picture, this study adds a number of critical new details to our previous work¹⁶, and can serve as a basis for future experimentation.

By transitioning from 2-D negative stain observations in the previous work to 3-D cryoEM in the present work, we both provide a much more native-like environment for the oligomers and gain a much more accurate count of the MBP tags in each oligomer through a larger population. This eliminates concerns that the staining process may have impacted the oligomeric structures, as well as challenges with accurately counting tags strictly from 2-D projections, where the counted components could overlap. Both cryoEM and EPR results point to significant flexibility and dynamics of the distal C-terminus of Vpu. Thus, the current study not only confirms with high confidence that in aqueous environment Vpu forms stable oligomers, but also reports for the first time on structural character of these oligomers.

Materials and methods

Protein constructs design, cloning, expression, and purification. In this study, we used three chimeric protein constructs of HIV-1 Vpu fused to maltose binding protein (MBP), which are MBP-Vpu full length (MBP-FL Vpu), MBP-Vpu with truncated Vpu helices 2 and 3 (MBP-Vpu- Δ h2h3), and MBP-Vpu with truncated helix 3 (MBP-Vpu- Δ h3). The MBP-FL Vpu was the same as one used previously¹⁶. The truncated constructs were generated by introducing a stop codon after amino acids R31 and G54, respectively, in the DNA of FL Vpu. The DNAs encoding all MBP-Vpu variants were cloned in the bacterial expression vector (pET15b) at NcoI/BamHI cloning sites. High-throughput prokaryotic expression vectors obtained after cloning, i.e., MBP-FL Vpu (MBP-Vpu)/pET15b, MBP-Vpu- Δ h2h3/pET15b, MBP-Vpu- Δ h3/pET15b were used further for protein expression. For cloning, protein expression, and purification by double-affinity chromatography, i.e., Nickel (Ni^{2+} , Ni)-affinity chromatography and amylose affinity chromatography, the previously developed protocols¹⁶ were utilized.

The purity of all proteins was assessed by using sodium dodecyl sulfate gel electrophoresis (SDS-PAGE) and western blotting (WB), as described in Majeed et al.¹⁶.

Assessing the protein oligomeric state using size exclusion chromatography. We used size exclusion chromatography (SEC) to assess the oligomerization state of the purified MBP-FL Vpu, MBP-Vpu Δ h2h3, and MBP-Vpu Δ h3 proteins, as described previously. A buffer composed of 50 mM sodium phosphate (NaPi) pH 7.4, 150 mM NaCl, 200 μ M TCEP and 10% glycerol was used to equilibrate the column prior to protein sample injection. Then 500 μ L of protein sample was injected into the column and eluted by running a SEC program with 0.5 ml/min flow rate. For these experiments, we used a Superdex™ 200 increase 10/300 GL size-exclusion column (GE Healthcare) plugged into an AKTÄ explorer 100 (Amersham Biosciences) protein purifier system.

CryoEM grid preparation and data acquisition. Purified MBP-FL Vpu at concentration of 10 μM in a buffer solution containing 25 mM Tris pH 7.4, 150 mM NaCl and 100 μM TCEP was used in cryo-EM experiments. Quantifoil® R 1.2/1.3 Holey Carbon on copper or gold 200 mesh grids were used for vitrification of MBP-FL Vpu. Grids were negatively glow discharged at 15 μA for 20 s using a PELCO EasiGlow™. 3.5 μl of protein sample was applied to the grids in the humidity-controlled chamber of FEI Mark IV Vitrification Robot. The grids were then blotted on both sides for 1.5 to 2 s and plunged into liquid ethane to vitrify.

The MBP-FL Vpu data was collected at the Baylor College of Medicine Cryo-EM ATC using a Thermo Fisher™ Glacios™ Cryo-transmission electron microscope, operated at 200 keV. The data was collected with a Falcon 4 direct electron detector in counting mode, at a magnification of 120,000, corresponding to a pixel size of 1.2 Å. The dose rate was set to 5.44 e^- per Å² per second. Data was collected using ThermoFisher EPU software. A total of 478 micrographs were collected in a single session.

CryoEM data processing. The raw movie frames were aligned for motion correction in RELION4.0¹⁹. Motion-corrected images were then imported to EMAN2²⁰ suite for processing. Image processing followed standard EMAN2 single particle reconstruction pipeline²¹, cross-validated using RELION4.0 as outlined briefly below.

Roughly 20,000 putative particles were selected using deep learning-based particle picking in EMAN2²². False positives were manually removed to produce a final set of 14,657 particles used for all subsequent analyses.

128 class averages were produced using the bispectrum-based unsupervised class averaging method in EMAN2. The class averages were then used to generate an initial model by stochastic gradient descent for 3-D refinement. Particles were refined using standard refinement with “gold standard” resolution estimate²³. 3-D refinement was also performed using RELION4.0 for cross validation purposes, with good agreement when using the EMAN2 starting model. Multiple additional refinements were attempted using several different starting models and multi-model refinement methods. Multi-model refinement²⁴ into 4 classes produced two distinct structures. The particles associated with these two structures were then independently refined producing the two maps shown in Fig. 3. A newer GMM variability method²⁵ was also applied, and identified the same discrete separation of the data into two groups, along with local variability at the level of roughly the 25 Å resolution achieved in the refinements. The resolution of these maps is not limited by raw image quality, which clearly extended to subnanometer resolution, but rather to the remaining conformational variability of the assemblies within the two identified subsets.

Estimating the number of monomers in the self-associated protein oligomers based on cryoEM structures. Since the major densities observed in the 3-D map are strikingly similar in size to the known MBP structure, the number of monomers in the complex was determined by simply docking into each of the masses of appropriate size in each map. At this resolution, structures lack sufficient features to determine subunit orientations with any level of accuracy. Maps are presented as isosurfaces, and significant size variations are possible with different choices for isosurface level. To determine an appropriate isosurface level for docking and visual presentation, the PDB structure of MBP was converted to an electron density map at similar resolution, then the isosurface was selected such that the contained mass agreed with the PDB mass using the standard protein density of 1.35 g/ml (0.81 Da/Å³)²⁵. The isosurface of the cryoEM map was then adjusted such that individual docked subunit volumes roughly match the size of the PDB-based monomer structure. An additional transparent isosurface is presented at a lower threshold in Fig. 4 to show some of the weaker densities present in the structure representing higher variability regions. As an additional internal control, the volume ratio of the MBP to undocked density in the cryoEM maps is consistent with the relative mass ratio of MBP to Vpu within the margin of error. This increases our confidence that the observed oligomer consists of 6 MBPs. While the larger of the two observed structures arguably has sufficient overall mass to account for 7 MBP/Vpus there isn't an ideal docking location for a seventh MBP in this structure. Much of the additional mass seems disordered.

Protein spin labeling and EPR spectroscopy. Two MBP-Vpu single cysteine mutants labeled with MTS spin label as previously¹⁶ were used in EPR experiments. The mutations Q36C and N55C were located in the C-terminus of Vpu on opposite sides of Helix 2. Amino acid numbering is that for FL-Vpu.

Continuous wave (CW) EPR experiments were done in the Georgieva lab at TTU with an X-band Bruker EMXmicro spectrometer. The EPR spectra were recorded at room temperature using magnetic field modulation amplitude of 1.5 to 2 Gauss and 0.5 mW microwave power.

Pulse dipolar EPR (PDS) experiments used standard four-pulse double electron–electron resonance, DEER^{26–28}, and six-pulse DQC²⁶. Both were conducted at ACERT (Cornell University) at 60 K using a home-built Ku-band pulse EPR spectrometer operating at MW frequency around 17.3 GHz^{29,30}. DEER experiment setup³¹ used for electron spin-echo detection a $\pi/2$ - π - π pulse sequence with 32 ns π -pulse widths applied at the low-field edge of the nitroxide spectrum. A 16 ns pump π -pulse was tuned to 70 MHz lower frequency, pumping at the central peak of the spectrum. A 32-step phase cycle³² suppressed all unwanted echo contributions to the signal and some other instrumental artifacts, leaving only three unwanted dipolar pathways produced by the 4-pulse DEER sequence³³. Nuclear electron spin-echo envelope modulation (ESEEM) caused by the matrix protons was suppressed by summing up the data traces recorded in four sequential measurements where initial pulse separations and the start time of detection were advanced in subsequent measurement by 9.5 ns that is by a quarter period of the 26.2-MHz nuclear Zeeman frequency of protons at 0.615 T corresponding to 17.3 GHz working frequency³⁴.

DQC experiments (conducted on N55C) used 6-pulse sequence with 6 ns π -pulses and 64-step phase cycle isolating the dipolar signal. No unwanted dipolar pathways are generated in this sequence. The short distances

between the labels produced very fast dipolar evolution appearing as a narrow peak in the center of the symmetrical in time dipolar signal. An apparent small background was due to dipolar couplings between spin labels at longer distances as can better be seen in DEER data. The additive background contribution is most likely very small in this case and can be left in place to be processed together with the main part of the dipolar signal.

Primary echo decays were routinely recorded for all samples. Supporting Fig. 1 shows echo decays for both mutants in protonated and deuterated buffers.

Some of time-domain DEER data traces $V(t)$ were processed to distances. All traces were conditioned using standard approaches^{26,31,35,36} and then reconstructed into distance distributions $P(r)$'s by either Tikhonov regularization method or an SVD application accessible via ACERT website. The DEER signal record $V(t)$ was corrected for the decay caused by intermolecular dipole–dipole couplings by fitting the latter points (about half of the record) of $\ln[V(t)]$ to the straight line extrapolated to zero time and subtracted from $\ln[V(t)]$, giving the antilog $u(t) = d(t) + 1$, where $d(t)$ is contributed by the dipolar evolution of DEER signal. Then, $u(t)$ normalized as $u(t)/u(0)$ gives typical presentation of DEER data, (cf. Fig. 6). Another data form, $v(t) = d(t)/u(0)$ gives background-free “dipolar” data used as an input in reconstructing distances between the coupled electron spins. The DEER data for the two spin-labeled residues are shown in Supporting Figs. 2 and 3.

Results

The Vpu soluble oligomers are a result of Helix 1 (TM) self-association. To establish with certainty which region of Vpu contributes to its oligomerization in solution, in addition to MBP-FL Vpu, we produced two truncated versions of Vpu that are MBP-Vpu Δ h3 and MBP-Vpu Δ h2h3 (with deletions of either Helix 3 or both Helices 2 and 3). We studied these protein versions with SEC and found that all MBP-Vpu variants elute as oligomers of close molecular weight (Fig. 2). MBP-Vpu oligomers were formed even when both Helices 2 and 3 were deleted, although the corresponding elution peak at 8.5–12 ml was broader than the elution peaks of MBP-FL Vpu and MBP-Vpu Δ h3. The estimated full width at half maximum (FWHM) for these peaks were 0.74, 0.85 and 1.5 (in ml), respectively, for the FL Vpu, Vpu Δ h3, and Vpu Δ h2h3. The observed elution peak broadening for Vpu lacking both Helix 2 and Helix 3 possibly indicates that just Helix 1 is insufficient for stabilizing the Vpu oligomers, leading to increased heterogeneity in the oligomeric order. However, increased hydrophobic interactions between Vpu and column beads due to more exposed Vpu Helix 1 cannot be ruled out as a reason for the broadening of the SEC peak. Still, no complete oligomer disassembly occurs, as the intensity of the SEC elution peak at 16–18 ml remains unchanged (Fig. 2). On the other hand, a little if any difference was observed in the SEC profiles of MBP-FL Vpu and MBP-Vpu Δ h3, suggesting the essential role of protein region comprising Helice 1 and likely Helix 2 in Vpu self-association and oligomer stabilization, which is in agreement with what was proposed for Vpu oligomer in lipid environment¹².

As we reported previously, the assessed by SEC MBP-Vpu oligomers have a molecular weight greater than 200 kDa and elute well after the void volume for the SEC column we used (Supporting Fig. 1)¹⁶.

While it seems unlikely that soluble MBP could induce oligomerization which would not otherwise occur, we performed an additional test, fusing MBP to another single-span viral membrane protein, namely the coronavirus E protein (Supporting Fig. 2). No oligomerization was observed in the E protein-MBP system.

CryoEM describes the overall structure of the stable, soluble MBP-FL Vpu oligomers. In a previous study, we utilized nsEM to observe stable soluble oligomers of MBP-Vpu¹⁶. These oligomers were typically formed at protein concentrations exceeding 5 μ M, which indicated that cooperative mechanisms may have contributed to this process. In this study MBP-FL Vpu oligomers were imaged using cryoEM to confirm that the well-defined soluble oligomers observed by nsEM are reproducible under solution-like cryoEM conditions. The cryoEM freezing process occurs on a ms timescale, which is too fast for water to crystallize or for slower processes such as oligomer disassembly, to occur³⁷, thereby effectively providing a time snapshot of the solution conformation. This reduces concerns that the staining process may have impacted oligomerization.

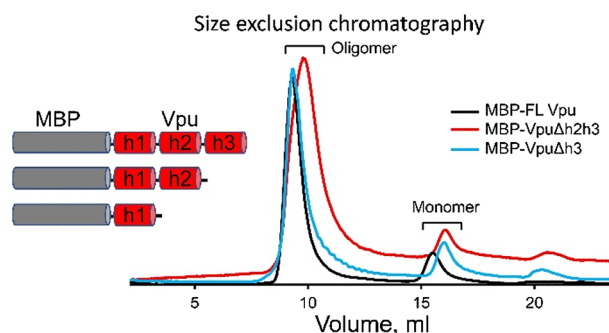


Figure 2. Results from SEC on MBP-Vpu protein in buffered aqueous solution. The SEC results demonstrate that all the MBP-FL Vpu, MBP-Vpu Δ h3 and MBP-Vpu Δ h2h3 constructs form oligomers, as they elute predominantly at about 8.5–12 ml (depending on the construct) and only small fraction elutes as monomers corresponding to the peak at 16–18 ml. The protein concentration was 15 μ M for all the three constructs.

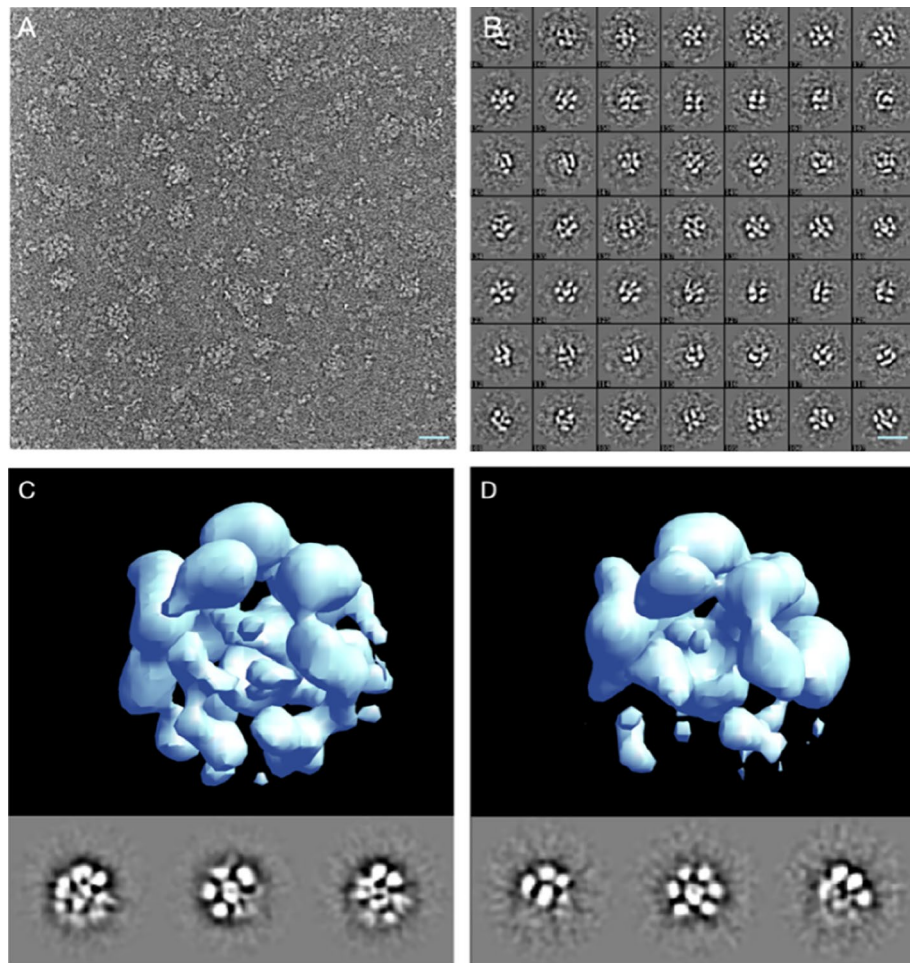


Figure 3. Single particle cryoEM analysis of MBP-FL Vpu soluble oligomers. (A) A micrograph showing representative oligomers and dissociated monomers; (B) representative unsupervised 2-D class averages from 14,657 particles; (C,D) single-particle reconstruction of the two identified particle populations with 11,541 (C) and 2815 (D) respectively. The three images below each 3-D map are the 3 orthogonal projections of the map, making the lower density regions easier to observe. The scale bar is 20 nm.

To perform structural analysis by single-particle cryoEM, purified MBP-FL Vpu protein was used. The oligomerization of MBP-FL Vpu in buffer solution was confirmed by SEC (Fig. 2) prior to cryoEM imaging. CryoEM data collected in the present study had sufficient contrast to enable clear visualization of oligomeric proteins in the raw micrographs (Fig. 3A). A representative micrograph containing MBP-Vpu oligomers, and reference-free 2D class averages are shown in Fig. 3A and B, respectively. The micrograph exhibits mostly oligomeric assemblies similar to those previously observed in nsEM¹⁶, but a small fraction of lower order oligomers and possibly monomers were also present. Notably, the majority of the self-associated protein particles were of a visually similar size, and only a very small fraction of non-specific larger aggregates were observed. When further analyzed, the visibly uniform particles readily group into unsupervised 2-D classes of a similar size implying a self-consistent quaternary structure of size-limited protein oligomers.

To confirm whether the 2-D class-averages represent different views of a single 3-D quaternary structure or represent multiple states, we conducted de-novo reconstructions using EMAN2¹⁹, performing several cross-validations and classification steps. The analysis produced two self-consistent 3-D structures at low resolution (~25 Å), representing different populations of the observed particles. Out of a total of 14,657 particles, about 80% were associated with one larger-size structure (shown in Fig. 3C) with several low-intensity features, whereas the remaining about 20% of the particles correspond to a similar, but slightly smaller-size structure (Fig. 3D). The large densities in the periphery of these structures are the correct size to be MBP domains, with the density in the center (Figs. 3C and D), presumably correspond to the Vpu TM oligomer. The variable lower densities observed further from the core (Fig. 3D) can be attributed to the distal Vpu C-terminal helices.

We made attempts to further classify the particles or characterize the remaining variability in the system not accounted for in the two classes by using a deep-learning Gaussian Mixture Model (GMM) approach²⁵. However, this effort did not yield useful insights beyond confirming the overall positioning of the major densities in both structures with persisting variability at the level of the ~25 Å resolution. This level of variability is entirely reasonable, and expected. The MBP domains are serving as markers to permit counting the number of self-associated

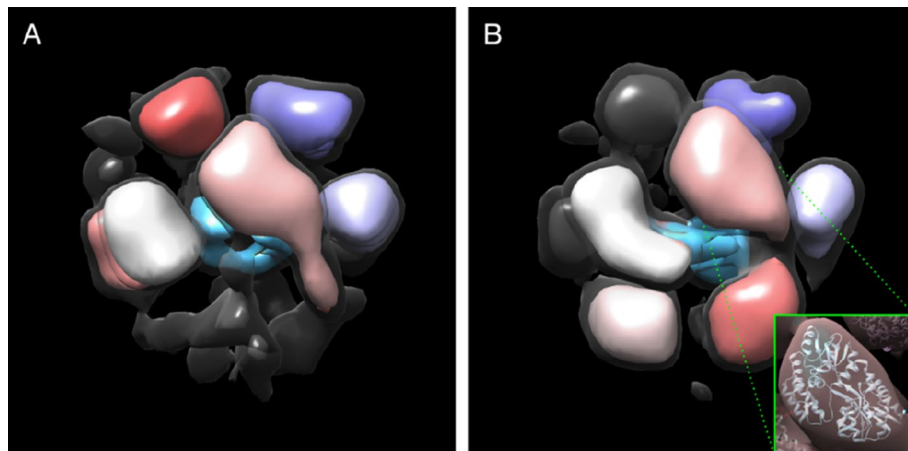


Figure 4. Modeling the oligomeric state of MBP-FL Vpu. (A,B) Maps of the two oligomeric states with populations of 80% and 20% are shown in Fig. 3C and D, respectively. The regions where MBP could be docked are colored in pink, gray, shades of purple, and red. The electron density, which most likely represent Vpu oligomerization core is colored in blue. Views are from different angle than those in Fig. 3. A lower isosurface threshold presented in transparent gray shows the lower-density connections in the reconstruction. The inset shows an MBP molecule (PDB: 1PEB) docked into the pink density region of the 3D model as a representative example.

Vpus in an oligomer, and their packing would naturally be highly variable, constrained only by the limited space available at the appropriate distance from the core. Even if the oligomerization core of Vpus were fairly ordered, the core is far too small to drive the cryoEM image alignment process and produce a high-resolution structure.

The two maps are shown again in Fig. 4 at two different isosurface thresholds to visualize the lower and higher density regions simultaneously. The density attributed to the Vpu core is shown in blue at the core of the structure. The remaining colored densities are the similarly sized/shaped MBP domains. Six of the MBP domains can be readily docked into both maps. The map from the larger 80% population map has sufficient total volume to accommodate a 7th MBP, but the associated extra domain in the map is somewhat smaller than the other MBP domains at the same threshold. Our best interpretation is that, when present, the 7th MBP is more flexible than the remaining MBPs leading to more motion averaging and a somewhat smaller apparent size. While the resolution of the 3-D maps is clearly not sufficient to build any sort of model of the oligomerization domain, estimates of the mass of the core can be made based on volume measurements normalized using the larger MBP domains, and this mass estimate is consistent with the MBP-derived count of 6–7 Vpus in each oligomer. Docking of MBP into one of the subunit densities is shown in an inset in Fig. 4B simply to show that the overall size/shape agrees. This should not be interpreted as having a robust orientation for each MBP.

Protein spin labeling and EPR spectroscopy confirm that the distant C-terminus of Vpu is highly dynamic.

Before undertaking full-fledged multi-site spin labeling EPR experiments to map protein dynamics and solve spatial organization of monomers in the Vpu oligomer, we limited this task to using two carefully selected spin-labeled sites. We used the previously generated single cysteine mutant Q36C¹⁶ in the linker at the beginning of Helix 2 N-terminal side and added new labeling site N55C in the linker connecting Helix 2 to Helix 3 (Fig. 5A). The residues selected for EPR studies are located far from the MBP moiety of MBP-Vpu, thus we believe they are not affected by the presence of MBP. Therefore, we studied these residues in the context of FL MBP-Vpu for consistency with the cryoEM data and data analyses.

The broad CW EPR spectrum recorded for spin-labeled Q36C mutant (Fig. 5B) reinforced the previous conclusion that this protein region has restricted motional dynamics¹⁶. This is in line with the SEC results showing that the linker connecting Helices 1 and 2 play a role in Vpu soluble oligomer stabilization. This may require specific structural arrangement of the protein region containing residue 36. Could be that this linker is ordered, possibly in contact with the oligomer-forming Helices 1. On the other hand, the CW EPR spectrum for the spin-labeled residue N55C has narrow lines (Fig. 5B), indicating that this protein region is highly mobile and possibly unstructured^{38–42}, in agreement with the structures of monomeric Vpu C-terminal (Fig. 5A)^{43,44}. While a minor population of protein with restricted motional dynamics at this site contributing broad low-intensity lines to the EPR spectrum of this spin-labeled residue cannot be entirely ruled out, such was not immediately apparent in the signal, which is clearly dominated by the high-intensity lines of the predominant conformation.

The pulse EPR (DEER) data for the Q36C mutants were previously published¹⁶. It was of more interest to conduct DEER distance measurement for the newly spin-labeled residue N55C, probing conformations of this protein region. For the DEER measurements of this mutant, we used partial or full solvent deuteration by substituting H₂O for D₂O and glycerol for glycerol-*d*₈ in the buffer aiming to increase the signal and extend the upper range of measurable distances at least for more water exposed spin-labeled sites due to increased spin label phase memory relaxation time, T_m ^{45–47}.

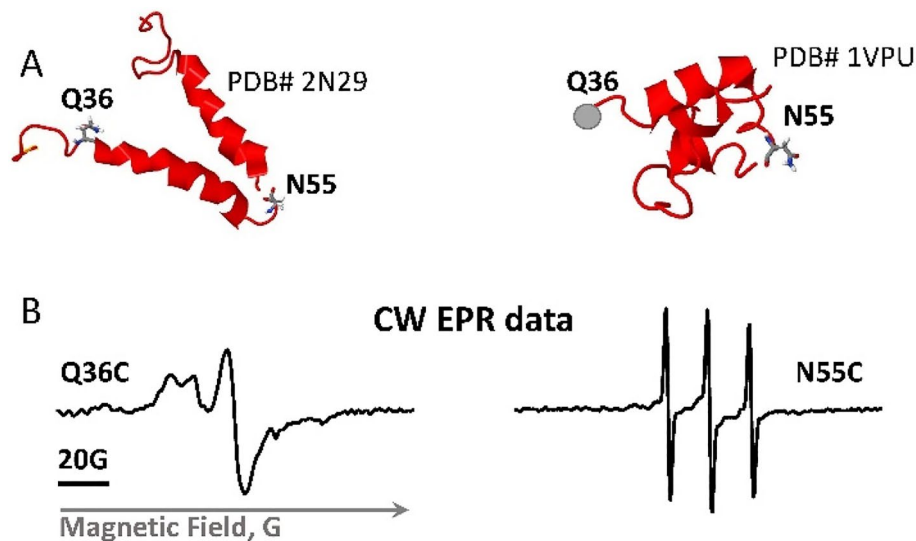


Figure 5. Vpu spin labeling and CW EPR results. (A) Shown are two NMR structures of the soluble C-terminal domain of the Vpu protein with the residues mutated to cysteines and spin-labeled. The residue Q36C is located at the beginning of amphipathic Helix 2, residue N55C is in highly dynamic loop connecting Helices 2 and 3. (B) EPR spectra of spin-labeled residues Q36C and N55C show very different mobility of spin labels at these sites.

Unlike Q36C¹⁶, N55C is favorable to spin labeling. Long T_m 's and larger primary echo amplitude compared to Q36C (Supporting Information) show that this residue is more accessible to the aqueous phase. The two recorded DEER traces for spin-labeled mutant N55C and evolution times of 1 μ s and 3 μ s (Fig. 6A) revealed very different form-factors of signal decays. The clearly bimodal character of DEER signal trace for the shorter evolution time (t_m) and the respective distance distribution are shown in Figs. 6B and C. For the 3 μ s data, however, one can see what appears mostly as a slow “uniform” background with a small narrow feature in the beginning of the record. To produce such signal in a spin pair widely distributed distance above 80 Å would be necessary⁴⁸.

These observations suggest that spin labels in close proximity or at moderate distances in Fig. 6C and D have shorter relaxation times than a fraction of labeled sites, which may be located far away from these apparent spin clusters by the nature of the oligomeric assembly. They could be residing on less restricted “floppy” domains, so that only small dipolar evolution occurs on a limited time-scale. For long evolution times these slowly-relaxing spins-labels contribute most of the echo signal and long distances due to these sites dominate the DEER signal. It is unlikely that these slow decays are caused by intermolecular spin interactions since oligomer spin clusters are confined to widely separated complexes. In such cases analogues to spin-labeled micelles, intermolecular contributions to DEER signal are small⁴⁸.

This result suggests that the Vpu region containing the loop between Helices 2 and 3, and possibly Helix 3, are sampling multiple conformations outside the Vpu oligomer core. This is in line with cryoEM results (Figs. 3 and 4) indicating that this protein region is not well resolved, implying significant variability.

However, in addition to this broadly distributed distances, for the residue N55C we also observed a measurable contribution of very short inter-spin distances at or below 10 Å reported by double quantum coherence (DQC)⁴⁹, as shown in Fig. 6D. Apparently, these very short distances correspond to a not yet quantified fraction of labels occupying sites locked in distinct conformations. They possibly contribute broad and difficult to quantify lines in the EPR spectrum of residue N55C in Fig. 5B. Based on these results, we may conclude that some of Helices 2 and possibly Helices 3 from different protomers interact with each other and/or the oligomeric core, bringing into proximity the residues N55 in the Vpu oligomer. This could explain the presence of peripheral low electron densities in the cryoEM structures seen in Fig. 3D. These results may direct future approaches to finding more specific details on helix organization in Vpu oligomers.

Discussion

Vpu is a HIV-1 encoded accessory protein, which has been linked to several processes important for the virus functions in the infected cells^{4, 6, 50, 51}. However, at present, the Vpu structures underlying these functions are not fully characterized. In cellular membranes, Vpu is thought to function in both oligomeric and monomeric states¹⁰, but the factors governing the observed quaternary structure variations have not been adequately identified and studied. Furthermore, we¹⁶ and others¹³ found that this protein can form soluble oligomers outside of the hydrophobic membrane environment. This is atypical behavior for a transmembrane protein, although other such proteins alternating between soluble and membrane-bound functional states are known^{17, 18}. It may well be that the observed soluble oligomers of Vpu are purely a result of fortuitous physicochemical properties, as currently there is insufficient evidence to confirm or rule out their physiological relevance. One plausible role could be that soluble oligomers serve to transport this protein between cellular compartments or as a vehicle to transport other cellular material in non-orthodox ways. In our quest to both better understand the Vpu

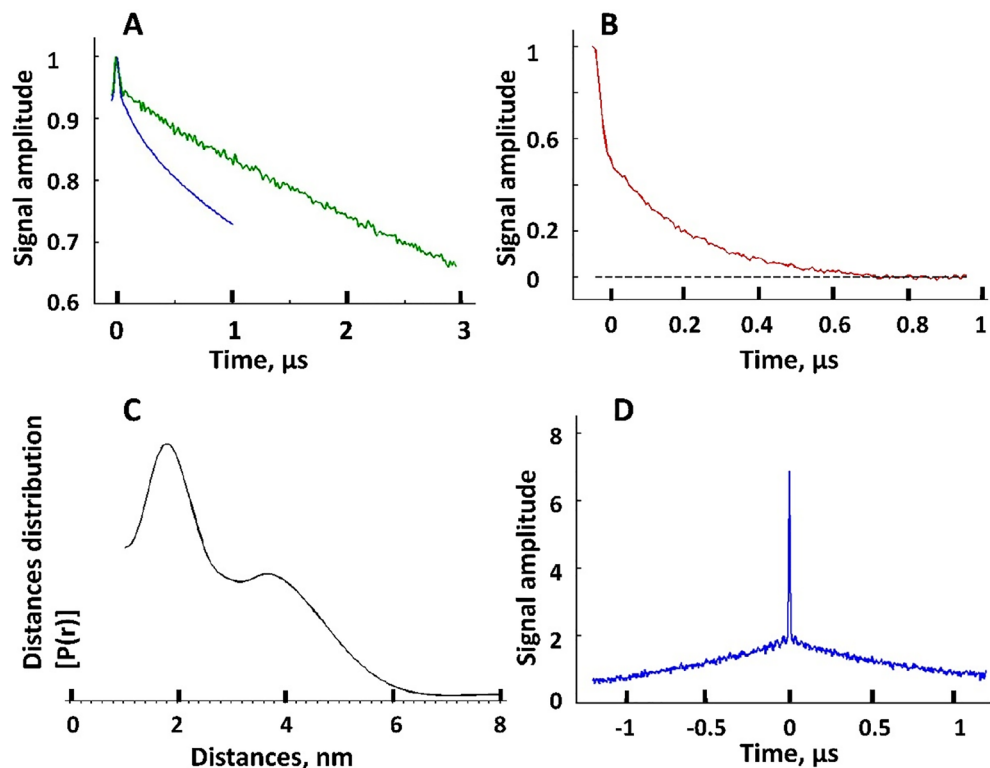


Figure 6. The DEER data and reconstructed inter-spin distances for Vpu spin-labeled at residue N55C. (A) Raw DEER data recorded for two different evolution times, 1 μs (blue) and 3 μs (green). (B) Background subtracted DEER signal for 1 μs evolution time data in (A). The black dashed line indicates the zero-signal amplitude. (C) The reconstructed inter-spin distances for the data in (B). (D) The intense narrow peak in DQC data originates from very short distances on the order of 10 \AA for some spin-labels at N55C in Vpu oligomer. These distances are too short to be sensed by DEER whose sensitivity rolls off quickly below 20 \AA .

oligomers as well as develop techniques for better studying such unusual assemblies, we utilized a combination of several experimental techniques: cryoEM, EPR, SEC and protein engineering. Given that FL Vpu monomers have a molecular weight of only about 9 kDa, to maximize the protein size-sensitive cryoEM studies, we made use of MBP to provide a stable tag with sufficient mass for visualization. These higher mass MBP-Vpu constructs achieve sufficient size for easy cryoEM visualization. A similar approach has been used previously in cryoEM studies of small proteins^{52, 53}, and MBP is quite soluble and known not to form oligomers on its own⁵⁴. While the structures clearly possess some level of structural variability, the obtained cryoEM data were sufficiently self-consistent to build a 3-D structural model of MBP-Vpu oligomers. These results were consistent with oligomers with a minimum of 6 Vpu subunits, with a possible population with 7 subunits. These oligomerization numbers have not been observed previously and may indicate that Vpu may not necessarily form distinct symmetric oligomers. But the fact that it can serve as a stable binding core for a much more massive soluble protein coat is interesting in itself, as such objects may promise new biomedical applications and mechanisms and could have other useful properties. We also found that the oligomer formation is a result of Vpu TM self-association, and Helix 2 has stabilizing effect, as observed by SEC. It is not yet known how the regions of TMs are structured in the Vpu oligomer as the task is inherently complex, particularly because no homology modeling is available and the oligomer may not necessarily be symmetric, rendering models like in Fig. 7 below naïve. Additional approaches, such as laborious development of EPR single and double-label mapping strategies will be required to resolve these issues. However, in this limited EPR study CW EPR and DEER data based on the singly spin-labeled residue N55C in Vpu C-terminal domain indicated that this Vpu region is highly dynamic, sampling a wide range of conformations, and the labeled sites at the C-termini of protein protomers are mostly widely separated. It also could be result of heterogeneous assembly such as a complex of smaller oligomers or anti-parallel helix bundling, all complicating factors to finding approaches for PDS structure mapping. While the structure of the Vpu core oligomer would not be completely out of reach for modern CryoEM methods at roughly 50 kDa, this would only be possible if the entire oligomer were rigid and structurally homogenous, which does not appear to be the case.

Thus, the results from this and previous studies provided unambiguous evidence that Vpu forms well-defined and stable oligomers in solution and its exact structure may be a subject of a future study. Further studies, could provide more information on the structure of these oligomers and could possibly serve as a ground to uncover a physiological function linked to them.

Based on the results from this study, we can consider a model of Vpu soluble oligomers in which the regions of Helices 1 self-associate to form a hydrophobic core of possibly a hexameric quaternary structure, which is

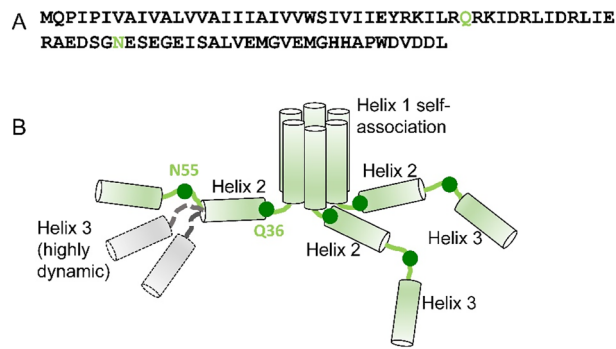


Figure 7. Proposed model of the soluble Vpu oligomers. **(A)** Amino acid sequence of FL Vpu drawn with Helices 2 pulled of Helices 1. The linker between Helix 1 and Helix 2 is highlighted in gray, and the residue Q36 is in green. **(B)** Hexameric arrangement of Vpu monomers: Helices 1 from six protomers come together to form the oligomer core. The linker between Helix 1 and Helix 2, and Helix 2 in each protomer are arranged in a way to stabilize the oligomer. The residues Q36 and N55 are shown as dark green circles. The residue Q36 is possibly oriented toward the oligomer core and occluded. Possibly, the Helix 2 is in even closer proximity to the oligomerization core to screen it from water environment. Helix 3 is widely spread and conformationally heterogeneous. Helices 2 and 3 for only three protomers are shown for clarity. Helix 3 is highly dynamic and heterogeneous in conformation—Possible alternative conformations of this Vpu region are shown for just one protomer for the sake of clarity. Also, for the clarity of representation, the model shown here does not account for the possible interactions between Helices 1 and 2 and Helices 3 from neighboring Vpu protomers.

further stabilized by the favorable arrangement of amphipathic Helices 2 and linkers between Helix 1 and Helix 2 of each protomer (Fig. 7) possibly covering the Helix-1 formed core. The linker between Helices 1 and 2 is possibly occluded, which could explain the difficulties to spin label the residue Q36C, as well as the obtained slow-motional CW EPR and DEER data for this residue¹⁶. Helices 3 may predominantly splay and be highly dynamic.

It is also interesting to mention that a previous study found that the phosphorylation of Ser 52 and Ser 56 in Vpu polypeptide enhances the protein oligomerization in detergent⁵⁵. However, our results in solution suggest that such phosphorylation is not essential, as under our experimental conditions the equilibrium was shifted exclusively toward stable FL Vpu oligomers and the oligomerization was unaffected when the region containing Ser 52 and 56 was deleted (Fig. 2). The observed differences might be a result of an altered Vpu conformation in detergent vs. solution.

Vpu has previously been considered exclusively a transmembrane protein and several NMR studies reported on its monomeric structure and oligomerization in lipid environment, with a pentamer proposed as the most probable quaternary organization^{56–58}. In addition, we previously observed Vpu oligomer restructuring upon transition from soluble to lipid-bound state¹⁶. Therefore, it is quite likely that the oligomeric organizations of Vpu in lipid and in solution are not identical, taking into account that the interactions between Vpu hydrophobic Helices 1 in aqueous solution and in lipid environment participate in vastly different interactions⁵⁹.

Data availability

The cryoEM datasets generated and/or analysed during the current study are not publicly available as they are too large to be placed in the supplement but are available from the corresponding authors Steven J. Ludtke and Elka R. Georgieva on reasonable request.

Received: 16 May 2023; Accepted: 1 September 2023

Published online: 06 September 2023

References

- Mitchell, R. S. *et al.* Vpu antagonizes BST-2-mediated restriction of HIV-1 release via beta-TrCP and endo-lysosomal trafficking. *PLoS Pathog.* **5**, e1000450 (2009).
- Roy, N., Pacini, G., Berlioz-Torrent, C. & Janvier, K. Mechanisms underlying HIV-1 Vpu-mediated viral egress. *Front. Microbiol.* **5**, 177 (2014).
- Strebel, K., Klimkait, T. & Martin, M. A. A novel gene of HIV-1, vpu, and its 16-kilodalton product. *Science* **241**, 1221–1223 (1988).
- Gonzalez, M. E. Vpu protein: The viroporin encoded by HIV-1. *Viruses* **7**, 4352–4368 (2015).
- Khan, N. & Geiger, J. D. Role of viral protein U (Vpu) in HIV-1 infection and pathogenesis. *Viruses* **13**, 1466 (2021).
- Dube, M., Bego, M. G., Paquay, C. & Cohen, E. A. Modulation of HIV-1-host interaction: Role of the Vpu accessory protein. *Retrovirology* **7**, 114 (2010).
- Cohen, E. A., Terwilliger, E. F., Sodroski, J. G. & Haseltine, W. A. Identification of a protein encoded by the vpu gene of HIV-1. *Nature* **334**, 532–534 (1988).
- Strebel, K., Klimkait, T., Maldarelli, F. & Martin, M. A. Molecular and biochemical analyses of human immunodeficiency virus type 1 vpu protein. *J. Virol.* **63**, 3784–3791 (1989).
- Ramirez, P. W. *et al.* Plasma membrane-associated restriction factors and their counteraction by HIV-1 accessory proteins. *Cells* **8**, 1020 (2019).
- Hussain, A., Das, S. R., Tanwar, C. & Jameel, S. Oligomerization of the human immunodeficiency virus type 1 (HIV-1) Vpu protein—a genetic, biochemical and biophysical analysis. *Virol. J.* **4**, 81 (2007).

11. Langer, S. *et al.* HIV-1 Vpu is a potent transcriptional suppressor of NF-kappaB-elicited antiviral immune responses. *Elife* <https://doi.org/10.7554/eLife.41930> (2019).
12. Ma, C. *et al.* Expression, purification, and activities of full-length and truncated versions of the integral membrane protein Vpu from HIV-1. *Protein Sci.* **11**, 546–557 (2002).
13. Maldarelli, F., Chen, M. Y., Willey, R. L. & Strebel, K. Human immunodeficiency virus type 1 Vpu protein is an oligomeric type 1 integral membrane protein. *J. Virol.* **67**, 5056–5061 (1993).
14. Neil, S. J., Sandrin, V., Sundquist, W. I. & Bieniasz, P. D. An interferon-alpha-induced tethering mechanism inhibits HIV-1 and Ebola virus particle release but is counteracted by the HIV-1 Vpu protein. *Cell Host Microbe* **2**, 193–203 (2007).
15. Neil, S. J., Zang, T. & Bieniasz, P. D. Tetherin inhibits retrovirus release and is antagonized by HIV-1 Vpu. *Nature* **451**, 425–430 (2008).
16. Majeed, S. *et al.* Insights into the oligomeric structure of the HIV-1 Vpu protein. *J. Struct. Biol.* **215**, 107943 (2023).
17. Hsu, Y. T., Wolter, K. G. & Youle, R. J. Cytosol-to-membrane redistribution of Bax and Bcl-X(L) during apoptosis. *Proc. Natl. Acad. Sci. U.S.A.* **94**, 3668–3672 (1997).
18. Lesieur, C., Vecsey-Semjen, B., Abrami, L., Fivaz, M. & Gisou van der Goot, F. Membrane insertion: The strategies of toxins (review). *Mol. Membr. Biol.* **14**, 45–64 (1997).
19. Scheres, S. H. RELION: Implementation of a Bayesian approach to cryo-EM structure determination. *J. Struct. Biol.* **180**, 519–530 (2012).
20. Tang, G. *et al.* EMAN2: An extensible image processing suite for electron microscopy. *J. Struct. Biol.* **157**, 38–46 (2007).
21. Bell, J. M., Chen, M., Baldwin, P. R. & Ludtke, S. J. High resolution single particle refinement in EMAN2.1. *Methods* **100**, 25–34 (2016).
22. Bell, J. M., Chen, M., Durmaz, T., Fluty, A. C. & Ludtke, S. J. New software tools in EMAN2 inspired by EMDatabank map challenge. *J. Struct. Biol.* **204**, 283–290 (2018).
23. Henderson, R. *et al.* Outcome of the first electron microscopy validation task force meeting. *Structure* **20**, 205–214 (2012).
24. Ludtke, S. J. Single-particle refinement and variability analysis in EMAN2.1. *Methods Enzymol.* **579**, 159–89 (2016).
25. Chen, M. & Ludtke, S. J. Deep learning-based mixed-dimensional Gaussian mixture model for characterizing variability in Cryo-EM. *Nat. Methods* **18**, 930–936 (2021).
26. Borbat, P. P. & Freed, J. H. Pulse dipolar electron spin resonance: Distance measurements. *Struct. Inf. Spin-Labels Intrinsic Paramagn. Cent. Biosci.* **152**, 1–82 (2014).
27. Jeschke, G. DEER distance measurements on proteins. *Annu. Rev. Phys. Chem.* **63**, 419–446 (2012).
28. Milov, A. D., Ponomarev, A. B. & Tsvetkov, Y. D. Modulation beats of signal of double electron-electron resonance in spin echo for biradical systems. *J. Struct. Chem.* **25**, 710–713 (1984).
29. Borbat, P. P., Georgieva, E. R. & Freed, J. H. Improved sensitivity for long-distance measurements in biomolecules: Five-pulse double electron-electron resonance. *J. Phys. Chem. Lett.* **4**, 170–175 (2013).
30. Borbat, P. P., Crepeau, R. H. & Freed, J. H. Multifrequency two-dimensional Fourier transform ESR: An X/Ku-band spectrometer. *J. Magn. Reson.* **127**, 155–167 (1997).
31. Jeschke, G. & Polyhach, Y. Distance measurements on spin-labeled biomacromolecules by pulsed electron paramagnetic resonance. *Phys. Chem. Chem. Phys.* **9**, 1895–1910 (2007).
32. Gamliel, D. & Freed, J. H. Theory of 2-dimensional ESR with nuclear modulation. *J. Magn. Reson.* **89**, 60–93 (1990).
33. Borbat, P. P. & Freed, J. H. Pulse dipolar ESR: Distance measurements. In *Structure and Bonding* Vol. 152 (eds Timmel, C. R. & Harmer, J. R.) 1–82 (Springer Heidelberg, 2014).
34. Tang, S. G. *et al.* Structural basis for activation, assembly and membrane binding of ESCRT-III Snf7 filaments. *Elife* <https://doi.org/10.7554/eLife.12548> (2015).
35. Borbat, P. P. & Freed, J. H. Measuring distances by pulsed dipolar ESR spectroscopy: Spin-labeled histidine kinases. *Methods Enzymol.* **423**, 52–116 (2007).
36. Jeschke, G. DEER distance measurements on proteins. *Ann. Rev. Phys. Chem.* **63**, 419–446 (2012).
37. Cabra, V. & Samsó, M. Do's and don'ts of cryo-electron microscopy: A primer on sample preparation and high quality data collection for macromolecular 3D reconstruction. *J. Vis. Exp.* <https://doi.org/10.3791/52311> (2015).
38. Cooper, R. S., Georgieva, E. R., Borbat, P. P., Freed, J. H. & Heldwein, E. E. Structural basis for membrane anchoring and fusion regulation of the herpes simplex virus fusogen gB. *Nat. Struct. Mol. Biol.* **25**, 416–424 (2018).
39. Georgieva, E. R., Xiao, S., Borbat, P. P., Freed, J. H. & Eliezer, D. Tau binds to lipid membrane surfaces via short amphipathic helices located in its microtubule-binding repeats. *Biophys. J.* **107**, 1441–1452 (2014).
40. Georgieva, E. R. Nanoscale lipid membrane mimetics in spin-labeling and electron paramagnetic resonance spectroscopy studies of protein structure and function. *Nanotechnol. Rev.* **6**, 75–92 (2017).
41. Torricella, F., Pierro, A., Mileo, E., Belle, V. & Bonucci, A. Nitroxide spin labels and EPR spectroscopy: A powerful association for protein dynamics studies. *Biochim. Biophys. Acta Proteins Proteom.* **1869**, 140653 (2021).
42. McHaourab, H. S., Steed, P. R. & Kazmier, K. Toward the fourth dimension of membrane protein structure: Insight into dynamics from spin-labeling EPR spectroscopy. *Structure* **19**, 1549–1561 (2011).
43. Zhang, H., Lin, E. C., Das, B. B., Tian, Y. & Opella, S. J. Structural determination of virus protein U from HIV-1 by NMR in membrane environments. *Biochim. Biophys. Acta* **1848**, 3007–3018 (2015).
44. Willbold, D., Hoffmann, S. & Rosch, P. Secondary structure and tertiary fold of the human immunodeficiency virus protein U (Vpu) cytoplasmic domain in solution. *Eur. J. Biochem.* **245**, 581–588 (1997).
45. Borbat, P. P., Georgieva, E. R. & Freed, J. H. Improved sensitivity for long-distance measurements in biomolecules: Five-pulse double electron-electron resonance. *J. Phys. Chem. Lett.* **4**, 170–175 (2013).
46. Georgieva, E. R. *et al.* Effect of freezing conditions on distances and their distributions derived from double electron electron resonance (DEER): A study of doubly-spin-labeled T4 lysozyme. *J. Magn. Reson.* **216**, 69–77 (2012).
47. Georgieva, E. R., Borbat, P. P., Ginter, C., Freed, J. H. & Boudker, O. Conformational ensemble of the sodium-coupled aspartate transporter. *Nat. Struct. Mol. Biol.* **20**, 215–221 (2013).
48. Borbat, P. P. *et al.* Conformational motion of the ABC transporter MsbA induced by ATP hydrolysis. *PLoS Biol.* **5**, e271 (2007).
49. Borbat, P. P., McHaourab, H. S. & Freed, J. H. Protein structure determination using long-distance constraints from double-quantum coherence ESR: study of T4 lysozyme. *J. Am. Chem. Soc.* **124**, 5304–5314 (2002).
50. Douglas, J. L. *et al.* Vpu directs the degradation of the human immunodeficiency virus restriction factor BST-2/Tetherin via a {beta}TrCP-dependent mechanism. *J. Virol.* **83**, 7931–7947 (2009).
51. Ewart, G. D., Sutherland, T., Gage, P. W. & Cox, G. B. The Vpu protein of human immunodeficiency virus type 1 forms cation-selective ion channels. *J. Virol.* **70**, 7108–7115 (1996).
52. Nygaard, R., Kim, J. & Mancina, F. Cryo-electron microscopy analysis of small membrane proteins. *Curr. Opin. Struct. Biol.* **64**, 26–33 (2020).
53. Coscia, F. *et al.* Fusion to a homo-oligomeric scaffold allows cryo-EM analysis of a small protein. *Sci. Rep.* **6**, 30909 (2016).
54. Selmke, B. *et al.* Open and closed form of maltose binding protein in its native and molten globule state as studied by electron paramagnetic resonance spectroscopy. *Biochemistry* **57**, 5507–5512 (2018).
55. Chen, C. P. *et al.* Membrane protein assembly: Two cytoplasmic phosphorylated serine sites of Vpu from HIV-1 affect oligomerization. *Sci. Rep.* **6**, 28866 (2016).

56. Lu, J. X., Sharpe, S., Ghirlando, R., Yau, W. M. & Tycko, R. Oligomerization state and supramolecular structure of the HIV-1 Vpu protein transmembrane segment in phospholipid bilayers. *Protein Sci.* **19**, 1877–1896 (2010).
57. Sharpe, S., Yau, W. M. & Tycko, R. Structure and dynamics of the HIV-1 Vpu transmembrane domain revealed by solid-state NMR with magic-angle spinning. *Biochemistry* **45**, 918–933 (2006).
58. Park, S. H., De Angelis, A. A., Nevzorov, A. A., Wu, C. H. & Opella, S. J. Three-dimensional structure of the transmembrane domain of Vpu from HIV-1 in aligned phospholipid bicelles. *Biophys. J.* **91**, 3032–3042 (2006).
59. Stangl, M. & Schneider, D. Functional competition within a membrane: Lipid recognition vs. transmembrane helix oligomerization. *Biochim. Biophys. Acta* **1848**, 1886–96 (2015).

Acknowledgements

We gratefully acknowledge Isaac Forrester for collecting the cryo-EM data used in this study. Oluwatosin Adetyui is acknowledged for participation in initial production of MBP-FL Vpu protein. The study was supported by start-up funds from the Department of Chemistry and Biochemistry at TTU (to ERG), NIH grant R01GM080139 to (SJL, Baylor College of Medicine), and NIH grant 1R24GM146107 to National Biomedical Resource for Advanced ESR Techniques. (ACERT) at Cornell University. CryoEM data was collected at the Baylor College of Medicine CryoEM ATC, which includes equipment purchased under support of CPRIT Core Facility Award RP190602.

Author contributions

S.M.: experiment, data analysis and interpretation, figures, writing the manuscript; L.D.: data analysis and interpretation, figures, writing the manuscript; M.M.I.: experiment, data analysis; O.I.: experiment; P.P.B.: experiment, data analysis and interpretation, figures, writing the manuscript; S.J.L.: supervision, funds acquisition, data interpretation, writing the manuscript; E.R.G.: conception, design, experiment, data analysis and interpretation, figures, writing the manuscript, supervision, funds acquisition. All authors contributed to and agreed with the final version of the manuscript.

Competing interests

Elka R. Georgieva is a member of the Scientific Reports Editorial Board. All the other authors have no competing interest.

Additional information

Supplementary Information The online version contains supplementary material available at <https://doi.org/10.1038/s41598-023-41873-0>.

Correspondence and requests for materials should be addressed to S.J.L. or E.R.G.

Reprints and permissions information is available at www.nature.com/reprints.

Publisher's note Springer Nature remains neutral with regard to jurisdictional claims in published maps and institutional affiliations.



Open Access This article is licensed under a Creative Commons Attribution 4.0 International License, which permits use, sharing, adaptation, distribution and reproduction in any medium or format, as long as you give appropriate credit to the original author(s) and the source, provide a link to the Creative Commons licence, and indicate if changes were made. The images or other third party material in this article are included in the article's Creative Commons licence, unless indicated otherwise in a credit line to the material. If material is not included in the article's Creative Commons licence and your intended use is not permitted by statutory regulation or exceeds the permitted use, you will need to obtain permission directly from the copyright holder. To view a copy of this licence, visit <http://creativecommons.org/licenses/by/4.0/>.

© The Author(s) 2023